Kawasaki disease and ENSO-driven wind circulation

Joan Ballester,[1,6] Jane C. Burns,[2] Dan Cayan,[3] Yosikazu Nakamura,[4] Ritei Uehara,[4] and Xavier Rodó[1,5]

[1] Kawasaki disease (KD) is the most common cause of acquired heart disease in children worldwide. Recently, a climatological study suggested that KD may be triggered by a windborne agent traveling across the north Pacific through the westerly wind flow prevailing at midlatitudes. Here we use KD records to describe the association between enhanced disease activity on opposite sides of the basin and different phases of the El Niño-Southern Oscillation (ENSO) phenomenon, via the linkage to these tropospheric winds. Results show that years with higher-than-normal KD cases in Japan preferentially occur during either El Niño Modoki or La Niña conditions, while in San Diego during the mature phase of El Niño or La Niña events. Given that ENSO offers a degree of predictability at lead times of 6 months, these modulations suggest that seasonal predictions of KD could be used to alert clinicians to periods of increased disease activity. **Citation:** Ballester, J., J. C. Burns, D. Cayan, Y. Nakamura, R. Uehara, and X. Rodó (2013), Kawasaki disease and ENSO-driven wind circulation, *Geophys. Res. Lett.*, *40*, 2284–2289, doi:10.1002/grl.50388.

1. Introduction

[2] Kawasaki disease (KD) is an acute, self-limited vasculitis that occurs in children of all ages. The leading paradigm for the etiology of KD is that an as yet unidentified agent enters through the upper respiratory tract and causes a dramatic immunologic response in certain genetically predisposed children [*Rowley et al.*, 2008; *Onouchi*, 2009]. Coronary-artery aneurysms also develop in 20–25% of cases, but their development is clinically silent in most cases and may be recognized only years later at the time of sudden death or myocardial infarction [*Burns and Glodé*, 2004]. This risk can be dramatically reduced by a timely diagnosis and treatment early in the course of the illness [*Newburger*, 1991]. Unfortunately, without a diagnostic test for KD, children continue to be misdiagnosed with other more benign rash/fever syndromes caused by viruses or bacterial toxins [*Anderson et al.*, 2005].

[3] Although presently there is not a demonstrated methodology that can forecast the year-to-year variability of the disease, some useful steps have been taken which may be helpful to assist clinicians. *Burns et al.* [2005] first described the seasonality of KD in Japan. *Rodó et al.* [2011] recently showed for Japan and San Diego that the high number of KD cases in winter is associated with the seasonal enhancement of low- and high-tropospheric wind currents that sweep from the Asian continent to these sites. An atmospheric window is thus opened from November to March, wherein strong westerly winds connect the Asian continent with Japan and further across the north Pacific to the west coast of the United States (Supplementary Figure 1). The increasing phase of the three major KD epidemics in Japan coincided with this seasonal window (Supplementary Figure 2). Note that the trans-Pacific wind connection shifted to higher or lower latitudes than in the climatology for some of the years with higher-than-normal disease numbers [*Rodó et al.*, 2011]. The discovery of these associations led to the hypothesis that KD is caused by a pathogen or environmental trigger associated with winds blowing from the Asian continent [*Rodó et al.*, 2011; *Frazer*, 2012; find further details in the Supplementary Material].

[4] Because El Niño-Southern Oscillation (ENSO) is the major source of interannual atmospheric variability globally, especially over the Pacific Ocean and adjacent continents [*Trenberth*, 1998; *Glantz*, 2001], we postulated that ENSO might be involved in the interannual variability of KD through year-to-year anomalies in this seasonal atmospheric pattern. Indeed, ENSO plays an important role in the interannual modulation of other diseases in other regions of the world, such as malaria [*Hashizume et al.*, 2009], dengue [*Cazelles et al.*, 2005], and cholera [*Pascual et al.*, 2000; *Rodó et al.*, 2002; *Koelle et al.*, 2005]. The warm (cold) phase of the ENSO phenomenon, namely El Niño (La Niña), is characterized by anomalous surface and subsurface warming (cooling) in the central and eastern tropical Pacific, and cooling (warming) in the western tropical Pacific. These patterns are associated with anomalies in the tropical and extratropical pressure configuration [*Ballester et al.*, 2011] and wind circulation [*Jochum et al.*, 2007], with a substantial degree of symmetry between the warm and cold phases [*Hoerling et al.*, 1997].

2. Data and Methods

[5] Ocean and atmosphere data were derived from the NOAA NCDC ERRSST v2 [*Smith and Reynolds*, 2004] and the NCEP/NCAR reanalysis [*Kalnay et al.*, 1996], respectively. A recursive Butterworth filter with cutoff period of 18 months [*Ballester et al.*, 2011] was used to calculate the

---

[1]Institut Català de Ciències del Clima (IC3), Barcelona, Catalonia, Spain.
[2]Department of Pediatrics, Rady Children's Hospital San Diego and UCSD, La Jolla, CA, USA.
[3]Climate, Atmospheric Science, and Physical Oceanography, Scripps Institution of Oceanography, UCSD and Water Resources Discipline, US Geological Survey, La Jolla, CA, USA.
[4]Department of Public Health, Jichi Medical University, Tochigi, Japan.
[5]Institució Catalana de Recerca i Estudis Avançats (ICREA), Barcelona, Catalonia, Spain.
[6]California Institute of Technology (Caltech), Pasadena, CA, USA.

Corresponding author: J. Ballester, California Institute of Technology (Caltech), 1200 E California Blvd, Pasadena, CA 91125, USA, Mail Code: 131–24. (joanballester@caltech.edu)
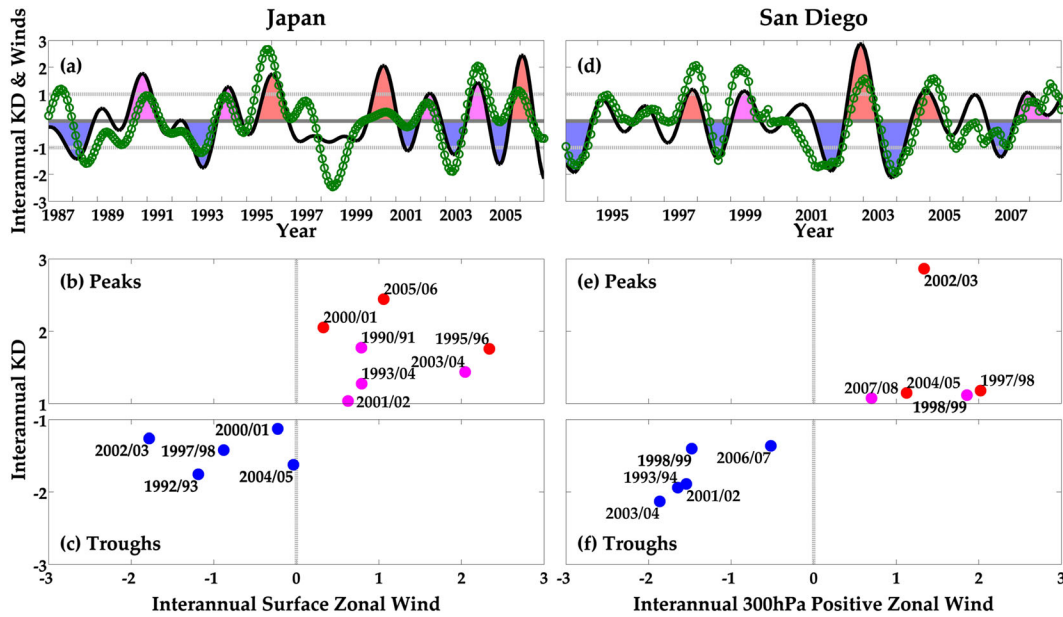
Figure 1. Relationship between atmospheric winds and KD in (a–c) Japan and (d–f) San Diego. Green curves in panels a and d depict the standardized (unitless) interannual component of surface zonal wind in Japan (130–135E, 40N) and 300 hPa positive zonal wind in the central north Pacific (170–150W, 10–45N), respectively. The positive zonal wind for a given month and region is here defined as the spatial average of only those grid points with positive interannual zonal wind anomalies (i.e., interannual easterly anomalies are excluded from the spatial average). Black lines in panels a and d correspond to the standardized (unitless) interannual component of monthly KD in Japan and San Diego, respectively. Note that correlations for time series in panels a and d are 0.61 and 0.76 (p < 0.001), respectively. Peaks (red and pink) and troughs (blue) reaching the ±1 standard deviation level are shaded. Peaks are grouped into two classes in order to separate among the different typologies of ocean-atmosphere patterns described in the manuscript. The correspondence between the standardized (unitless) interannual component of monthly KD with (b,c) surface zonal wind in Japan (130–135E, 40N) and (e,f) 300 hPa positive zonal wind in the central north Pacific (170–150W, 10–45N) is shown for the peaks (b,e) and troughs (c,f).

interannual component of detrended ocean and atmosphere variables. This component was then standardized, i.e., the local grid point mean was removed, and the difference was divided by the local grid point standard deviation. Standardized interannual anomalies of ocean and atmosphere data are shown in Figures 1–3 and Supplementary Figures 3 and 4.

[6] The interannual component of monthly KD time series was reconstructed with the use of an eigendecomposition analysis applied to the data covariance matrix (black line in Figures 1a and 1d). This reconstructed interannual component is explicitly used in Figures 1 and 3 and Supplementary Figures 3a and 3d. Find further details about the time series and the filtering in the Supplementary Material. The peaks and troughs reaching the ±1 standard deviation criterion in the reconstructed interannual component were analyzed in this study (red, pink, and blue events in Figures 1a and 1d). Composites of peaks (Figure 2 and Supplementary Figure 4) were computed as the average of the standardized interannual component of ocean and atmosphere variables for subsets of events. The criterion for the clustering of peaks is described in section 3.1 below.

3. Results

3.1. Ocean and Atmosphere Patterns Associated With Interannual KD Peaks

[7] The impact of tropical dynamics on extratropical variability is largely determined by the ocean surface temperature anomaly pattern within the tropical band. Warm anomalies in

the tropical oceans can alter the latent and sensible heat fluxes to the atmosphere, and thus the temperature and humidity above the ocean surface and the static stability and moisture flux convergence available for convection [*Chou and Chen*, 2010]. Tropical deep convection generates upper-level divergence, which alters the Hadley circulation and impacts the subtropics, as well as planetary-scale disturbances generating Rossby waves that propagate polewards in the subtropics and extratropics [*Hoskins and Ambrizzi*, 1993]. Given the impact of sea surface temperature anomalies on the tropospheric circulation in subtropical and extratropical latitudes, the redistribution of equatorial surface temperatures in the Pacific Ocean, and thus the phase of ENSO variability, is here used as the criterion for classifying the different typologies of KD peaks in Japan and San Diego.

[8] *Kug et al.* [2009] showed that equatorial warm anomalies during the mature phase of El Niño (La Niña) events, including those considered as El Niño Modoki [*Takahashi et al.*, 2011], were generally found to the east (west) of longitude 155E. Peaks in KD occurrence were thus clustered into two basic types (red and pink events in Figures 1a and 1d) according to the zonal range of anomalous equatorial warming (Supplementary Figures 3a and 3d). This longitudinal threshold provides a more comprehensive and precise characterization of the different ocean-atmosphere interactions and tropospheric teleconnections involved in the exacerbation of the disease (cf. columns in Figure 2 and Supplementary Figure 4). In the case of Japan, individual red peaks correspond to La Niña events or La Niña-like
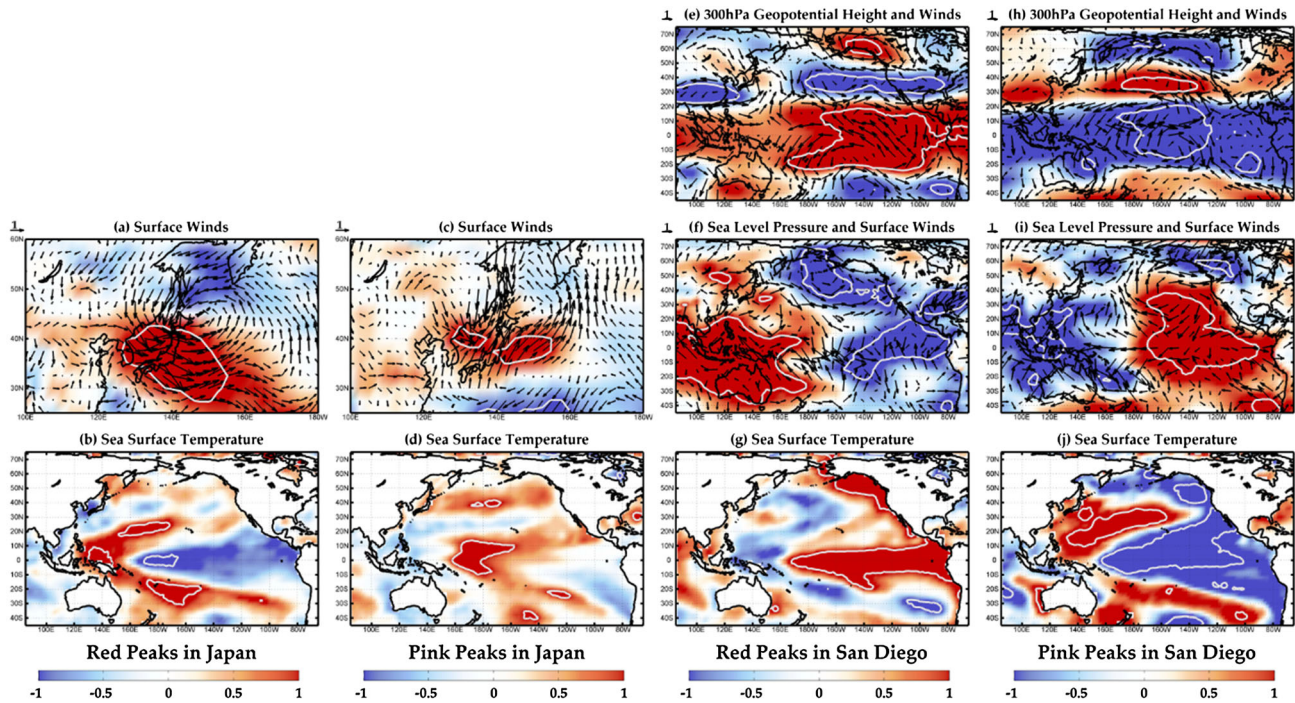
Figure 2. Ocean-atmosphere mean composites for the interannual peaks of KD in (a–d) Japan and (e–j) San Diego. From left to right, columns show the standardized (unitless) interannual anomalies for the peaks shown in red and pink in Figure 1a for Japan, and in red and pink in Figure 1d for San Diego. See the individual events in Supplementary Figures 3b and 3c, 3e and 3f, respectively. Maps correspond to the composites for surface zonal wind (shading and contours in Figures 2a and 2c), 300 hPa geopotential height (shading and contours in Figures 2e and 2h), 300 hPa winds (arrows in Figures 2e and 2h), sea level pressure (shading and contours in Figures 2f and 2i), surface winds (arrows in Figures 2a, 2c, 2f, and 2i), and sea surface temperature (shading and contours in Figures 2b, 2d, 2g, and 2j). White contours depict shaded areas with significant anomalies (p < 0.05).

conditions, with warm horseshoe-shaped anomalies in the western tropical Pacific (Supplementary Figure 3b), while pink peaks show warm anomalies in the central Pacific, mostly associated with early stages or the mature phase of El Niño Modoki events (Supplementary Figure 3c). In San Diego, individual red peaks correspond to central or eastern Pacific El Niño events or El Niño-like conditions (Supplementary Figure 3e), and pink peaks to La Niña events (Supplementary Figure 3f).

3.2. Patterns Favoring KD in Japan

[9] As a general rule of thumb, years with increased KD in Japan are associated with enhanced local low-troposphere westerly winds driven by a low pressure anomalous area centered to the north of Japan (Figures 2a and 2c), which corresponds to the westerly shift of the climatological Aleutian low (i.e., anticlockwise circulation at 180E, 50N in Supplementary Figure 1b). Note that the decrease in sea level pressure, and the subsequent strengthening of the westerly winds, are found for all the individual peaks (Figures 1a and 1b), and not just for the composite average, while anomalies of opposite sign are found for the whole set of troughs (Figures 1a and 1c). The low pressure and westerly wind anomalies corresponding to the peaks in Japan are in turn linked to ocean-atmosphere dynamics in the tropical Pacific. Warm ocean anomalies are thus observed in the western (120–160E, Figure 2b) or central (160E–160W, Figure 2d) tropical Pacific for all the peaks (Supplementary Figures 3a–c).

[10] Irrespective of the exact longitudinal position of the warm sea surface temperature anomaly, tropical convection and upper-level divergence are reinforced around 135–140E (i.e., same longitude as Japan), as a result of the coupling between the ocean and the overlying atmosphere. Note that the normal climatological pattern is for the Walker circulation in the tropical Pacific and the Hadley circulation in the western north Pacific to be particularly active in the boreal winter [*Wang*, 2005], and thus the zonal (Supplementary Figures 4b and 4e) and tropical-subtropical (Supplementary Figures 4c and 4f) cells become more pronounced. The enhancement of the northern Hadley circulation in the western Pacific ultimately strengthens the local westerly flow over Japan. In some cases, this strengthening is confined to the lower levels of the troposphere (i.e., below 700 hPa or ~3000 m; red shading in Supplementary Figure 4f), while in some other cases, it affects the whole column of air (Supplementary Figure 4c), further enhancing the eastern branch of the Asian jet stream in winter [*Hoskins and Ambrizzi*, 1993].

3.3. Patterns Favoring KD in San Diego

[11] Periods of higher-than-normal KD cases in San Diego are associated with the seasonally varying windborne atmospheric connection with continental Asia and Japan [*Rodó et al.*, 2011]. During the three most prominent peaks, decreased dynamic stability between 30N and 45N (Figures 2e and 2f) intensifies the westerly zonal winds in the subtropics along a direct zonal path at all vertical levels (Supplementary Figures 4j–l). On the other hand, during the other two major
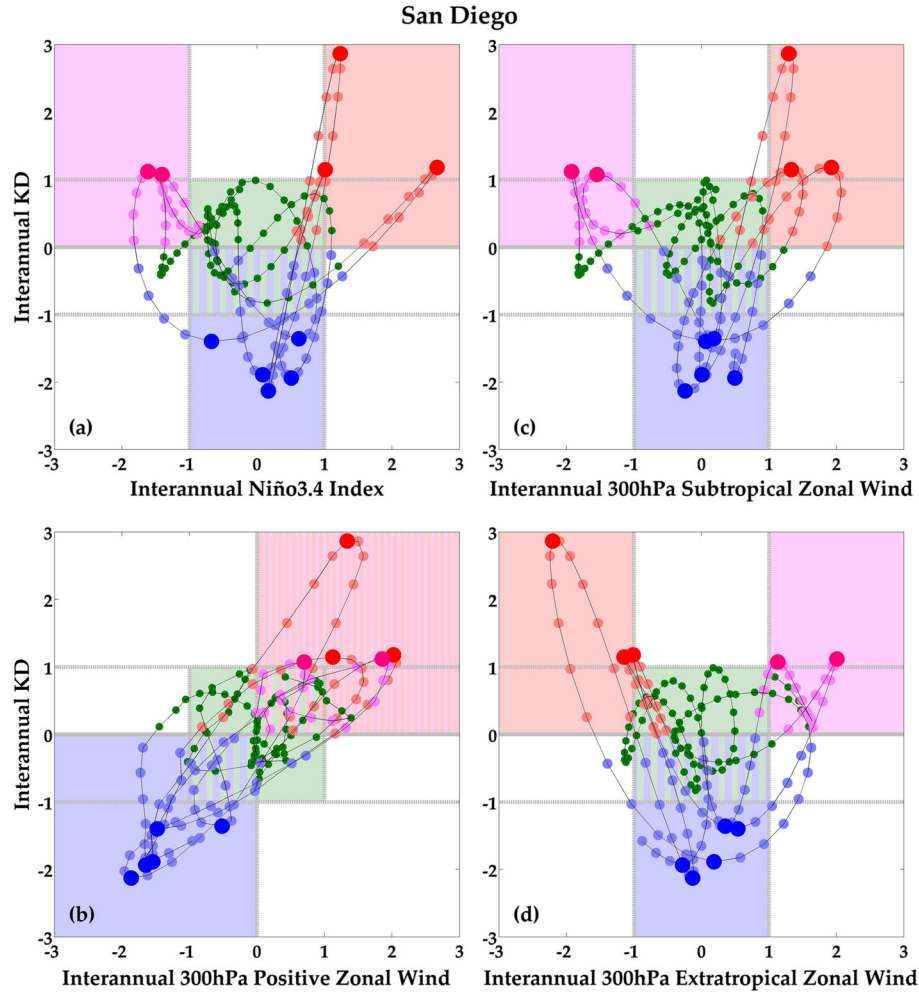
San Diego

Figure 3. Relationship between El Niño-Southern Oscillation variability and KD in San Diego. Correspondence between the standardized (unitless) interannual component of monthly KD in San Diego with (a) the monthly Niño3.4 Index (mean sea surface temperature in 170–120W, 5S–5N), (b) 300 hPa positive zonal wind in the central north Pacific (170–150W, 10–45N), and 300 hPa zonal wind in the (c) subtropical (150–145W, 20N), and (d) extratropical (150–145W, 45–50N) north Pacific. The positive zonal wind for a given month and region is here defined as the spatial average of only those grid points with positive interannual zonal wind anomalies (i.e., interannual easterly anomalies are excluded from the spatial average). Peaks and troughs are depicted in red, pink, and blue, respectively, and their increasing and decreasing phases (see the shading in Figure 1d) in light red, light pink, and light blue. Other months are shown in green.

peaks, this subtropical trajectory is weakened (Supplementary Figures 4p and 4r) as a result of increased dynamic stability developing in the central north Pacific (Figures 2h and 2i). Despite the weakening of the subtropical path in this second group of events, westerly winds are enhanced at midlatitudes, between 40 N and 55 N (Supplementary Figures 4p and 4q). Note that these two atmospheric configurations are nearly symmetric, corresponding to opposite ocean-atmosphere signatures of ENSO (Figure 3a), but both of them imply an increase of average westerly wind anomalies in the basin (Figure 3b), due to the enhancement of zonal winds in either the subtropics (Figure 3c) or extratropics (Figure 3d). Thus, the enhancement of the subtropical connection is explained by El Niño (Figure 2g), while the extratropical path is favored by La Niña (Figure 2j). On the other hand, troughs are linked to non-ENSO conditions (Figure 3a) and decreased average westerly wind anomalies in the basin (Figures 3b–d). Thus, even if each typology of peak is associated with a distinct ENSO-related ocean-atmosphere signature, increased

average westerly wind anomalies are found for all of them (Figures 1d and 1e), with anomalies of opposite sign for the set of troughs (Figures 1d and 1f).

[12] Particularly, in the first type of peak, the redistribution of temperatures, expressed as warming in the central and eastern tropical Pacific surface and subsurface, feeds back to the overlying wind and pressure configuration by weakening the Walker circulation, with decreased convection (subsidence) in the western (central and eastern) tropical Pacific and decreased surface (upper-troposphere) trade winds (westerly flows) in the central tropical Pacific (Supplementary Figure 4h). In addition, the warming in the central tropical Pacific reinforces the northern Hadley circulation (Supplementary Figure 4i), modifying the zonal circulation in the subtropics and at midlatitudes (Supplementary Figures 4k and 4l). The active convection resulting from the tropical warming also generates large-scale tropical-extratropical teleconnections, such as a wavetrain of pressure anomalies extending poleward and eastward in both

hemispheres [Figure 2e; *Karoly*, 1989; *Ballester et al.*, 2011], which in turn defines a set of alternative zonal wind anomalies throughout the north Pacific (Supplementary Figure 4j). Specifically, these anomalies produce a southward shift in the storm track associated with the subtropical jet stream [*Trenberth*, 1998], reinforcing the above mentioned connection at these latitudes between the Asian continent and San Diego. Instead, opposite pressure and wind anomalies are found during La Niña events. Thus, the Walker circulation is reinforced (Supplementary Figure 4n), and the northern Hadley cell in the central Pacific is weakened (Supplementary Figure 4o), leading to the strengthening of midlatitude westerly winds at all vertical levels (Supplementary Figures 4p and 4r).

4. Discussion and Conclusions

[13] Distinct patterns of coupled tropical ocean and atmosphere anomalies are found to modulate the atmospheric flow patterns across the north Pacific, and thus the interannual variations of KD on both sides of the north Pacific basin. These patterns operate to explain the mechanism described in *Rodó et al.* [2011], i.e., low-level zonal winds propagating the agent responsible for KD from the Asian continent to Japan, where the number of cases is especially high, and from there to north America through the free troposphere in an atmospheric bridge that crosses the whole north Pacific (Supplementary Material). A similar transmission mechanism is applicable for the seasonality (Supplementary Figure 1), the strong KD epidemics in the early portion of the Japan KD record (Supplementary Figure 2), and the interannual component of KD variability in Japan and San Diego. Note that *Smith* [2012] recently proved that a large number of biological agents are effectively transported from continental Asia to north America by tropospheric winds at different latitudes and heights throughout the north Pacific. The mechanism here found is in turn associated with an oceanic driving counterpart that operates via the ENSO phenomenon, and appears to support the robustness of the windborne line of evidence and the results obtained so far. In this sense, the role of the atmosphere in the modulation of the disease, and the identification now of a tropical Pacific set of linkages provides a physically coherent theory that explains a substantial portion of the variability of KD in distant, but climatically teleconnected regions across the north Pacific.

[14] Although the strengthening of zonal winds is the main common feature of all the periods with higher-than-normal KD in Japan and San Diego, interevent variability suggests that other processes may interfere with the tropical-extratropical interplay, such as extratropical variability modes, planetary waves, nonlinear feedbacks, or stochastic noise [*Trenberth*, 1997]. For example, periods of higher-than-normal KD in Japan are always associated with an enhancement of westerly winds in the lower troposphere (Figures 2a and 2c). Nevertheless, in the particular case of the red peaks in Figure 1a, the maximum tropical warming is observed at the same longitude than Japan (around 140E; Supplementary Figures 3a and 3b), and westerly winds are also enhanced in the middle and upper troposphere (Supplementary Figure 4c), thus favoring even more the transport of the agent to Japan. These factors might in turn explain the generally larger magnitude of KD anomalies for this typology of peaks (cf. red and pink maxima in Figure 1b). Interevent ocean-atmosphere

differences are however clearly larger for the case of San Diego, as a result of the major distance to the source region, which further complicates its characterization and generalization. Thus, the trans-Pacific wind trajectory across the subtropics (Figures 2e and 2f) is in some cases weakened and shifted to higher latitudes (Figures 2h and 2i), but these latter events again correspond to the peaks with the smallest KD anomalies (cf. red and pink maxima in Figure 1e). This result indicates a close correspondence between the enhancement of the climatological atmospheric mechanism and the magnitude of interannual KD anomalies.

[15] From a practical point of view, these results offer a new opportunity to develop a framework to predict seasonal KD activity, even without knowledge of the etiologic agent. The ability to predict periods of increased KD, especially in winter during the peak in the seasonality of the disease, will benefit from operational climate forecasting skill at time leads of 6 months in advance [*AchutaRao and Sperber*, 2006]. In particular, a KD forecasting method could take advantage of the performance of current state-of-the-art climate models and statistical schemes in the simulation and prediction of ENSO [*Chen et al.*, 2004] and derived atmospheric teleconnections in the north Pacific basin [*Wang*, 2009]. In this way, given the correspondence between disease numbers and zonal winds (Figure 1), predictions of KD anomalies could be made using climate forecasts of tropospheric circulation in the subtropics and extratropics. Similar methods are already implemented for other climate-related diseases. These forecasts might ultimately help physicians who must identify KD patients from among the hundreds of children with benign rash/fever symptoms.

References

AchutaRao, K., and K. R. Sperber (2006), ENSO simulation in coupled ocean–atmosphere models: are the current models better?, *Clim. Dyn.*, 27, doi:10.1007/s00382-006-0119-7.

Anderson, M. S., J. K. Todd, and M. P. Glodé (2005), Delayed Diagnosis of Kawasaki Syndrome: An Analysis of the Problem, *Pediatrics*, 115, doi:10.1542/peds.2004-1824.

Ballester, J., M. A. Rodríguez-Arias, and X. Rodó (2011), A new extratropical tracer describing the role of the western Pacific in the onset of El Niño: Implications for ENSO understanding and forecasting, *J. Climate 24*, doi:10.1175/2010JCLI3619.1.

Burns, J. C., et al. (2005), Seasonality and temporal clustering of Kawasaki syndrome, *Epidemiology*, 16, doi:10.1097/01.ede.0000152901.06689.d4

Burns, J. C., and M. P. Glodé (2004), Kawasaki syndrome, *Lancet*, 364, doi:10.1016/S0140-6736(04)16814-1.

Cazelles, B., M. Chavez, A. J. McMichael, and S. Hales (2005), Nonstationary Influence of El Niño on the Synchronous Dengue Epidemics in Thailand, *PLoS Med. 2*, e106, doi:10.1371/journal.pmed.0020106.

Chen, D., M. A. Cane, A. Kaplan, S. E. Zebiak, and D. Huang (2004), Predictability of El Niño over the past 148 years, *Nature 428*, doi:10.1038/nature02439.

Chou, C., and C. A. Chen (2010), Depth of Convection and the Weakening of Tropical Circulation in Global Warming, *J. Climate*, 23, doi:10.1175/2010JCLI3383.1.

Frazer, J. (2012), Infectious disease: Blowing in the wind, *Nature*, 484, doi:10.1038/484021a.

Glantz, M. H. (2001), *Currents of Change: El Niño's Impact on Climate and Society*, 194 pp., Cambridge University Press, Cambridge.

Hashizume, M., T. Terao, and N. Minakawa (2009), The Indian Ocean Dipole and malaria risk in the highlands of western Kenya, *Proc. Natl. Acad. Sci.*, *106*, doi:10.1073/pnas.0806544106.

Hoerling, M. P., A. Kumar, and M. Zhong (1997), El Niño, La Niña, and the Nonlinearity of Their Teleconnections, *J. Climate*, *10*, 1769–1786, doi:10.1175/1520-0442(1997)010<1769:enolna>2.0.co;2.

Hoskins, B. J., and T. Ambrizzi (1993), Rossby wave propagation on a realistic longitudinally varying flow, *J. Atmos. Sci.*, *50*, 1661–1671, doi:10.1175/1520-0469(1993)050<1661:RWPOAR>2.0.CO;2.

Jochum, M., C. Deser, and A. Phillips (2007), Tropical atmospheric variability forced by oceanic internal variability, *J. Climate*, *20*, doi:10.1175/JCLI4044.1.

Kalnay, E., et al. (1996), The NCEP/NCAR 40-Year reanalysis project, *Bull. Am. Meteorol. Soc.*, *77*, 437, doi:10.1175/1520-0477(1996)077<0437:TNYRP>2.0.CO;2.

Karoly, D. J. (1989), Southern Hemisphere circulation features associated with El Niño–Southern Oscillation, *J. Climate*, *2*, 1239–1252, doi:10.1175/1520-0442(1989)002<1239:SHCFAW>2.0.CO;2.

Koelle, K., X. Rodó, M. Pascual, M. D. Yunus, and G. Mostafa (2005), Refractory periods and climate forcing in cholera dynamics, *Nature*, *436*, doi:10.1038/nature03820.

Kug, J. S., F. F. Jin, and S. I. An (2009), Two Types of El Niño Events: Cold Tongue El Niño and Warm Pool El Niño, *J. Climate*, *22*, doi:10.1175/2008JCLI2624.1.

Newburger, J. W. (1991), and Coauthors. A Single Intravenous Infusion of Gamma Globulin as Compared with Four Infusions in the Treatment of Acute Kawasaki Syndrome, *N. Engl. J. Med.*, *324*, 1633–1639.

Onouchi, Y. (2009), Molecular genetics of Kawasaki disease, *Pediatr. Res.*, *65*, doi:10.1203/PDR.0b013e31819dba60.

Pascual M., X. Rodó, S. P. Ellner, R. Colwell, and M. J. Bouma (2000), Cholera Dynamics and El Niño-Southern Oscillation, *Science*, *289*, 1766–1769, doi:10.1126/science.289.5485.1766.

Rodó X., J. Ballester, D. Cayan, M. E. Melish, Y. Nakamura, R Uehara, and J.C. Burns (2011), Association of Kawasaki disease with tropospheric wind patterns, *Nat. Sci. Rep.*, *1*, doi:10.1038/srep00152.

Rodó, X., M. Pascual, G. Fuchs, and A. S. G. Faruque (2002), ENSO and cholera: A nonstationary link related to climate change?, *Proc. Natl. Acad. Sci.*, *99*, 12901–12906, doi:10.1073/pnas.182203999.

Rowley, A. H., S. C. Baker, J. M. Orenstein, and S. T. Shulman (2008), Searching for the cause of Kawasaki disease — cytoplasmic inclusion bodies provide new insight, *Nat. Rev. Microbiol.*, *6*, doi:10.1038/nrmicro1853.

Smith, T. M., and R.W. Reynolds (2004), Improved Extended Reconstruction of SST (1854–1997), *J. Climate*, *17*, doi:10.1175/1520-0442(2004)017<2466:IEROS>2.0.CO;2.

Smith, D. J. (2012), and Coauthors. Intercontinental Dispersal of Bacteria and Archaea in Transpacific Winds, *Appl. Environ. Microbiol.*, *79*, doi:10.1128/AEM.030297-12.

Takahashi, K., A. Montecinos, K. Goubanova, and B. Dewitte (2011), ENSO regimes: Reinterpreting the canonical and Modoki El Niño, *Geophys. Res. Lett.*, *38*, L10704, doi:10.1029/2011GL047364.

Trenberth, K. E. (1997), Short-Term Climate Variations: Recent Accomplishments and Issues for Future Progress, *Bull. Am. Meteorol. Soc.*, *78*, 1081–1096, doi:10.1175/1520-0477(1997)078<1081:STCVRA>2.0.CO;2.

Trenberth, K. E. (1998), and Coauthors. Progress during TOGA in understanding and modeling global teleconnections associated with tropical sea surface temperatures, *J. Geophys. Res.*, *103*, 14291–14324, doi:10.1029/97JC01444.

Wang, B. (2009), and Coauthors. Advance and prospectus of seasonal prediction: assessment of the APCC/CliPAS 14-model ensemble retrospective seasonal prediction (1980–2004), *Clim. Dyn.*, *33*, doi:10.1007/s00382-008-0460-0.

Wang, C. (2005), ENSO, Atlantic climate variability, and the Walker and Hadley circulations, in *The Hadley Circulation: Present, Past and Future*, edited by HF Diaz, RS Bradley, pp. 173–202, Springer, New York.